Extend the RTK Survey to GNSS-Denied Areas Using a Low-Cost Inertial-Aided Positioning Pole

Changxin Lai, Ruonan Guo, *Wuhan University*

BIOGRAPHY

Changxin Lai and Ruonan Guo are master's students at the *GNSS Research Center* and the *School of Geodesy & Geomatics*, *Wuhan University*, respectively. Their current research mainly focuses on inertial surveying and INS/GNSS integration algorithms.

ABSTRACT

The global navigation satellite system (GNSS) real-time kinematics (RTK) is a high-precision positioning technique that has been widely used as a versatile surveying tool. However, RTK becomes invalid in GNSS-denied areas due to signal blockage. The GNSS is thus often used in combination with inertial navigation system (INS) to obtain greater utility during GNSS signal outages, while GNSS/INS integrated systems still suffer from the rapid accumulation of INS navigation errors over time, especially for low-cost systems. In this work, we aim to extend the high-precision RTK positioning capability to GNSS-denied areas by using a low-cost inertial-aided positioning pole that contains a dollar-level inertial measurement unit (IMU) chip and an RTK receiver. The key to maintaining the positioning accuracy at an acceptable level is to manipulate the pole as a walking stick, in which case, the pole tip lands on the ground periodically. The pole tip velocity is zero when it maintains contact with the solid ground, and thus, lever-arm compensated zero-velocity updates (LA-ZUPTs) can be utilized to suppress INS navigation errors effectively in GNSS-denied areas. In addition, the coordinate updates (CUPTs) of RTK positioning are used at RTK-friendly positions to provide strict geometric constraints and reduce INS errors. Furthermore, INS-based filtering, along with a smoothing algorithm, is applied in postprocessing to further reduce the INS positioning error. Regularly aided by LA-ZUPTs and enhanced by the smoothing algorithm, the INS is able to maintain centimeter-level positioning accuracy in postprocessing when the operator walks through GNSS-denied areas over short distances. The experimental results show that the positioning accuracy can be maintained at 5 cm and 8 cm in terms of root-mean-square error (RMSE) for I-shaped surveying trajectories of 20 meters and L-shaped surveying trajectories of 20 meters through GNSS-denied areas, respectively. In addition, the combination of forward and reverse measurements can further improve the positioning robustness and lead to an accuracy improvement of over 40%. Therefore, it is feasible to use a low-cost inertial-aided positioning pole to bridge the GNSS gap and extend the RTK survey ability to GNSS-denied areas within a certain distance.

1 INTRODUCTION

With the development of global navigation satellite systems (GNSSs) and continuously operating reference stations (CORSs), real-time kinematics (RTK) has become a high-precision positioning technique that is widely applied in positioning, navigation and timing (PNT) applications. With great popularity in the surveying market, RTK positioning is generally accepted as a powerful surveying method, which is called an RTK survey. The typical RTK survey instrument is a 2-meter-high pole with a GNSS receiver at the top end and a spike at the bottom end, which is required to be placed vertically on the target point, and then its position is obtained by reducing the offset between the antenna phase center (APC) and pole tip. However, the satellite signal may be reflected or blocked by obstacles such as high walls, buildings and dense tree canopies, which are common in complex environments. These challenging environments that impact GNSS signals can induce multipath effect and limit the number of visible satellites, resulting in the degradation of RTK positioning. The worst situation, known as a GNSS outage or GNSS denial scenario, occurs when GNSS signals are unavailable, which may occur inside or between buildings or in a forested area. For such situations, RTK positioning is totally unavailable, making it difficult to obtain the accurate and reliable positions of targets in surveying [1].

Correspondingly, there is a traditional high-precision surveying instrument, a total station, which can be applied to measure the position of a target that is in a GNSS-denied area, but it requires intervisibility with targets and time-cost operations. In recent years, benefiting from integrated GNSS/INS navigation systems, tilted RTK with dollar-level inertial measurement units (IMUs) and advanced signal tracking technologies have emerged, which utilize the attitudes provided by RTK-aided INS initial alignment

solutions to obtain pole tip positioning with tilt compensation. Therefore, the applicability of high-precision RTK positioning can be extended to some restrictive environments [2]. For example, the availability of RTK-fixed solutions may increase by tilting the pole to increase the distance from the antenna to the building or wall to obtain more visible satellites and lower multipath interference. To some extent, tilting the pole can address the disadvantage of half-sheltered situations for RTK positioning, but it is still incapable of handling GNSS-denied environments such as surveying inside buildings, under bridges, or in forested areas. With the rapid development of microelectromechanical system (MEMS) IMUs, diversified product series have provided low-cost MEMS IMU modules and even chips with considerable precision and significant potential; therefore, MEMS-based inertial navigation systems (INSs), which provide high-frequency smoothed navigation information in terms of position, velocity and attitude with significant precision when aided by external information to reduce fast drift, have been widely used in various applications in navigation and engineering surveys [3], such as railway track surveying [4, 5] and pipeline surveying [6-8]. So is it possible to utilize a low-cost MEMS IMU to extend the positioning capability of the RTK survey instrument to GNSS-denied areas?

Inspired by the indoor pedestrian dead-reckoning (PDR) navigator using foot-mounted INS, where zero-velocity update (ZUPT) is available periodically at every step to correct the velocity error of PDR [9-12], we can mount a low-cost IMU on the pole tip and operate the pole like a walking stick to benefit from the periodic ZUPTs when the pole tip lands on the ground at every step. For a typical walking-stick-like manipulation, as depicted in Fig. 1, there are two different dynamic phases of pole manipulation: one is the flying phase, with the pole tip not contacting the ground; the other is the landing phase, with the pole tip landing on the ground and the pole body rotating around the pole tip. These two stages are alternating and repetitive when walking from the RTK fixed area to the GNSS-denied target points, so regular zero-velocity observations at the pole tip are available to restrict low-cost INS drift over time or distance. Such ZUPT-aided INS has a much slower positioning drift and can therefore extend the RTK survey capability during GNSS outages and obtain the coordinates of target points in GNSS-denied areas. In fact, the IMU does not have to be physically mounted on the pole tip but can be mounted anywhere on the pole and be projected to the tip through lever-arm compensation to conduct ZUPT, which can be called lever-arm compensated ZUPT (LA-ZUPT). Unlike traditional ZUPT, which requires the whole carrier, including the IMU, to remain stationary, LA-ZUPT refers to the concept of velocity update using zero velocity observations at any known point of a rigid body with a fully restrained connection to the IMU, regardless of IMU motion. This RTK extension solution is called INS/RTK with LA-ZUPT in this study. Correspondingly, the mentioned pole that extends RTK positioning to GNSS-denied areas is named the inertial-aided positioning pole. A similar idea has been applied in two patents, *Walking Stick Navigator for Position Determination* and *AINS Enhanced Survey Instrument*, with a ZUPT-aided tactical grade IMU mounted at the bottom of the pole [13, 14]. However, it requires a customized pole to obtain an IMU setup at the bottom of the pole, and the tactical grade IMU may be too expensive for RTK survey instruments. Therefore, we try to develop a low-cost GNSS-denied navigation solution with a dollar-level MEMS IMU chip mounted away from the bottom of the pole in order to explore other possibilities for flexible installation and acceptable cost.

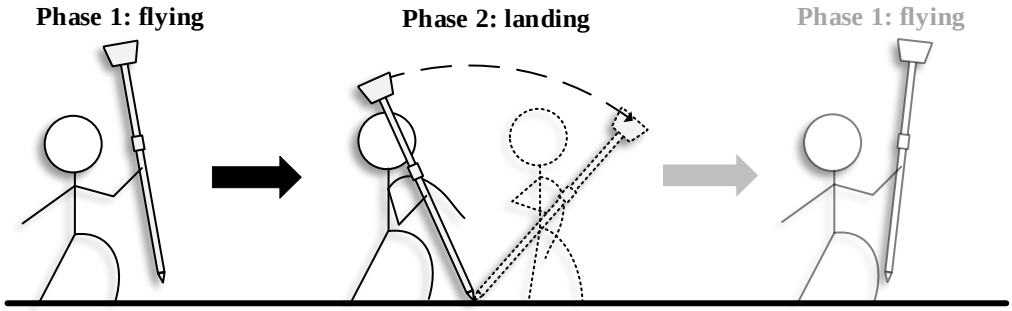

Fig. 1 Illustration of the typical motion of the positioning pole manipulated as a walking stick. (Note that in phase 2, the pole tip maintains contact with solid ground and its velocity is zero.)

In the solution of INS/RTK with LA-ZUPT, considering that postprocessing can be applied, the surveyor is required to ensure that the INS is initialized well with RTK positioning at the beginning and is corrected well by RTK positioning after walking through the GNSS-denied area to reach the end spot under open sky. In addition, as mentioned above, the pole must be manipulated as a walking stick during the GNSS outage to regularly conduct LA-ZUPT for the pole-mounted INS when the pole tip maintains contact with the solid ground. In terms of the data processing algorithm, the INS-based extended Kalman filter (EKF) is selected as the optimal estimator in terms of navigation states, including position, velocity and attitude, fusing the INS with RTK positioning or zero-velocity

measurement at the pole tip; furthermore, Rauch-Tung-Striebel (RTS) smoothing for postprocessing is adopted as a smoother to further reduce the error of the INS, with the goal of ensuring the reliable positioning ability of the inertial-aided positioning pole. Using INS aided by regular LA-ZUPT during GNSS outages, it should obtain much more accurate results than simply using a straightforward INS.

The remainder of this paper is organized as follows: Section 2 presents the workflow and algorithm of the proposed RTK extension solution, as well as some straightforward theoretical analysis. Then, Section 3 validates the feasibility of the proposed solution with multiple field tests in which several experiments are conducted to collect sufficient samples; the performance and result analysis are given from different perspectives. Finally, the conclusion of this study is given in Section 4.

2 METHODOLOGY

The proposed method aims to extend the RTK positioning capability to GNSS-denied cases by using an inertial-aided positioning pole. To achieve a desirable positioning accuracy, the typical surveying workflow is designed as follows:

1) Initially, manipulate the pole with sufficient movements in an open-sky environment to initialize the INS well with the aid of RTK positioning, and prepare to walk into the GNSS-denied area. Rapid and accurate heading alignment can be achieved in a short time according to our previous research [15].
2) Move along the survey trajectory by manipulating the pole as a walking stick in the GNSS-denied area, then place the pole tip exactly on the target point to be surveyed and keep the pole tip stationary for some time to carry out surveying while passing by.
3) Repeat step 2 at the next point of interest until an open-sky area is reached. Manipulate the pole with sufficient movements again at the end of the survey trajectory.
4) Reverse the survey trajectory and walk back to the starting point, if necessary.

The algorithm of the RTK extension solution is shown in Fig. 2. First, the aided INS requires initialization in terms of the initial position, velocity and attitude. The initial position and velocity of the INS can be easily provided by the GNSS RTK receiver in an open-sky environment, and coarse attitude initialization (i.e., coarse alignment) is performed by the accelerometer leveling process as well as the heading alignment method specific to low-cost MEMS IMUs [15]. Then, the inertial navigation algorithm is run; in addition, the INS-based extended Kalman filter works by integrating the INS navigation states with available external information, including the RTK positioning results and the mentioned zero-velocity observations at the pole tip, to correct the INS and restrict its drift. In addition to filtering, an RTS smoother is applied in postprocessing to obtain the globally optimal estimation of the INS error states and thereby further improve the INS precision. Finally, utilizing the corrected position and attitude of the INS as well as the lever-arm information, the coordinate of the pole tip landing on the target point is obtained by lever-arm compensation [2].

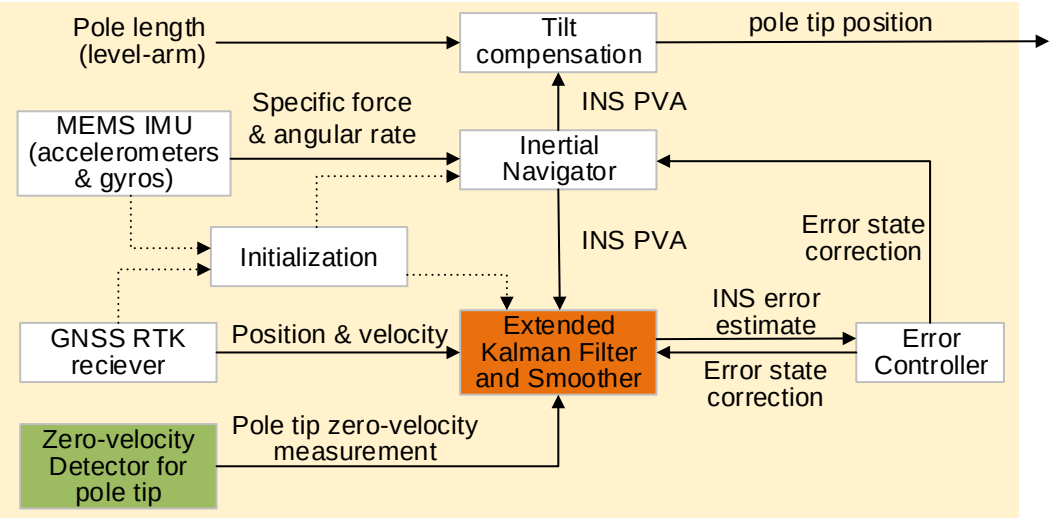

Fig. 2 Basic algorithm schematic of the proposed RTK extension solution

The core of the above algorithm of the RTK extension solution is to utilize the pole tip zero-velocity to perform LA-ZUPT in EKF, which estimates the INS error states and provides corrections to the INS during GNSS outages. As showed in **Fig. 3**, the velocity of the pole tip is calculated from the INS-indicated velocity with lever-arm compensation. It is clear that when the tip lands, its velocity is nearly zero despite the movement of the IMU being fixed in the middle of the pole. Thus, LA-ZUPT is feasible and applicable in this case. Compared with the conventional methods of using ZUPT, LA-ZUPT extends its applicability and makes ZUPT utilization more flexible.

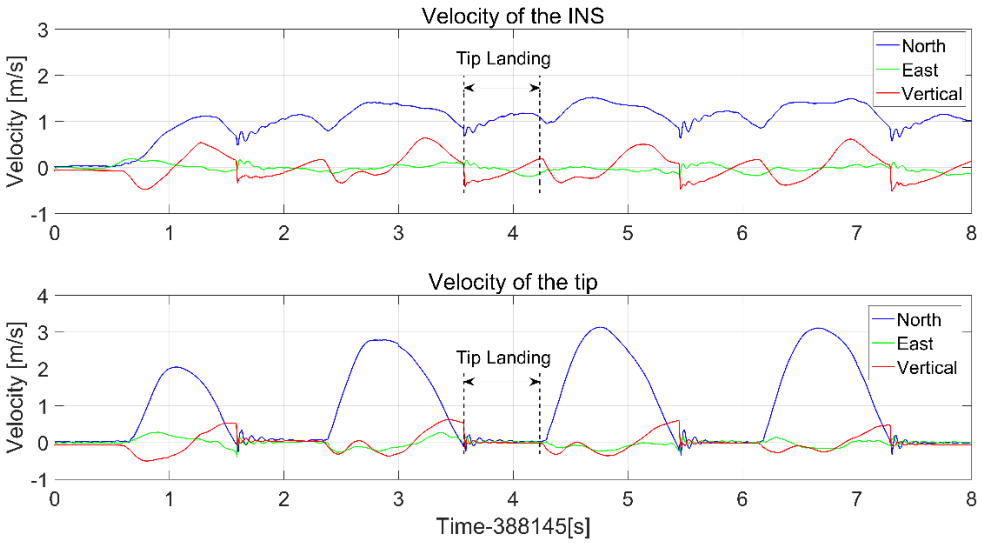

Fig. 3 Velocity comparison of the INS and the pole tip when the pole is manipulated as a walking stick. (Note that the pole tip landing on the ground is nearly stationary, while the INS mounted on the middle of the pole keeps moving.)

2.1 Implementation of the EKF and RTS

Details on the implementation of the INS mechanization and the EKF specification for low-cost IMUs can be found in [16]. As long as the coarse initialization of the INS is complete, the INS-based EKF begins to work with the INS for error estimation aided by external observations such as RTK positioning and pole tip zero-velocity. With a fine implementation of an EKF in terms of the system model and measurement model, the INS will obtain the appropriate correction and form a controlled system with closed-loop feedback [17].

2.2.1 System Model

Specifically for a low-cost MEMS chip and high dynamics of the pole that is manipulated as a walking stick, the INS error state vector of 21 dimensions in total is selected, which consists of basic 9-dimensional navigation state errors in terms of position errors, velocity errors and attitude errors in addition to the 12-dimensional residual IMU errors, including residual biases and scale factor errors of the gyroscopes and accelerometers, and it is defined as:

$$x = \left[(\delta r_{INS}^{n})^{T}\ (\delta v_{INS}^{n})^{T}\ \phi^{T}\ {b_g}^{T}\ {b_a}^{T}\ {s_g}^{T}\ {s_a}^{T}\right]^{T} \tag{1}$$

where the operator δ denotes the error of a variable, which means that δr_{INS}^{n} and δv_{INS}^{n} are the errors of position and velocity of the INS in the n-frame, respectively; ϕ refers to the attitude error defined in the phi angle model; b_g and s_g are the residual bias and scale factor errors of the gyroscopes, respectively; b_a and s_a are the residual bias and scale factor errors of the accelerometers, respectively. Next, the overall system model in continuous time form is expressed as:

$$\dot{x}(t) = \mathbf{F}(t)x(t) + \mathbf{G}(t)w(t) \tag{2}$$

where $\mathbf{F}(t)$ is the system matrix describing the system dynamics; $\mathbf{G}(t)$ is the system noise distribution matrix; and $w(t)$ is the system noise vector. To implement the system model, the time derivative of each state variable must be calculated. The perturbation of the position, velocity and attitude can be developed as follows [16]:

$$\begin{aligned} \delta\dot{r}^n &= -\omega_{en}^n \times \delta r^n + \delta\theta \times v^n + \delta v^n \\ \delta\dot{v}^n &= \mathbf{C}_b^n \delta f^b + \mathbf{C}_b^n f^b \times \phi - (2\omega_{ie}^n + \omega_{en}^n) \times \delta v^n \\ &\quad + v^n \times (2\delta\omega_{ie}^n + \delta\omega_{en}^n) + \delta g_l^n \\ \dot{\phi} &= -\omega_{in}^n \times \phi + \delta\omega_{in}^n - \mathbf{C}_b^n \delta\omega_{ib}^b \end{aligned} \tag{3}$$

where $\delta\theta$ is a rotation vector describing the misalignment of the computer frame with respect to the true n-frame; f^b is the specific force measured by the accelerometer, and δf^b refers to its error; $\delta\omega_{ie}^n$ and $\delta\omega_{en}^n$ denote the errors of ω_{ie}^n and ω_{en}^n, respectively; δg_l^n is the local gravity error in the n-frame; and ω_{in}^n is the angular velocity vector, where ω_{in}^n=$\omega_{ie}^n + \omega_{en}^n$ and $\delta\omega_{in}^n$ is its corresponding error. The INS error parameters, i.e., b_g, b_a, s_g and s_a, are modeled by the first-order Gauss-Markov process, described as:

$$\dot{x}_{GM}(t) = -\frac{1}{T_C} * x_{GM}(t) + w_{GM}(t) \tag{4}$$

where T_C is the correlation time of the process and $w_{GM}(t)$ is the driving white noise process [7]. Refer to [18] for more details regarding this stochastic process. Furthermore, the discrete system model, which is widely used, can be expressed as:

$$x_{k+1/k} = \mathbf{\Phi}_{k+1/k} * x_k + w_k \tag{5}$$

where $\mathbf{\Phi}$ is the state transition matrix and w is the process noise of the discrete system. They are given by:

$$\mathbf{\Phi}_{k+1/k} = \exp\left(\int_{t_k}^{t_{k+1}} \mathbf{F}(\tau)d\tau\right) \approx \mathbf{I} + \mathbf{F}(t_k)\Delta t \tag{6}$$

$$w_k = \int_{t_k}^{t_{k+1}} \mathbf{\Phi}(t_{k+1}, \tau)\mathbf{G}(\tau)w(\tau)d\tau \tag{7}$$

2.2.2 Measurement Model

In the modified EKF, the external information in terms of pole tip zero-velocity observations and RTK position observations is utilized for LA-ZUPT and coordinate update (CUPT), respectively. The overall system measurement model is denoted as:

$$z = \mathbf{H}x + n_v \tag{8}$$

where z is the measurement vector in terms of the velocity measurement and position measurement; $\mathbf{H}$ is the design matrix; x is the mentioned error state vector of the INS; and n_v is the measurement noise. The velocity measurement equation can be expressed as:

$$z_{ZUPT} = \hat{v}_{tip} - \tilde{v}_{tip} = \mathbf{H}_{ZUPT}x + n_v \tag{9}$$

where $\tilde{v}_{tip}$ is exactly the virtually 'measured' zero velocity at the pole tip, with $\tilde{v}_{tip} = [0\ 0\ 0]^T + n_{vT}$, and $\hat{v}_{tip}$ is the INS-indicated velocity at the pole tip obtained by velocity lever-arm compensation, as follows:

$$\hat{v}_{tip}^n = \hat{v}_{INS}^n + \hat{\boldsymbol{C}}_{\boldsymbol{b}}^{\boldsymbol{n}}\left(\hat{\omega}_{eb}^b \times l_{tip}^b\right) = \hat{v}_{INS}^n - (\omega_{ie}^n \times)\hat{\boldsymbol{C}}_{\boldsymbol{b}}^{\boldsymbol{n}} l_{tip}^b - \hat{\boldsymbol{C}}_{\boldsymbol{b}}^{\boldsymbol{n}}\left(l_{tip}^b \times\right)\hat{\omega}_{ib}^b \tag{10}$$

where $\hat{v}_{INS}^n$ is the INS velocity; l_{bT}^b is the lever arm from the INS to the pole tip; $\hat{\omega}_{eb}^b$ is the angular rate of the e-frame relative to the b-frame in the b-frame, which can be separated into the angular rate of the e-frame relative to the i-frame in the b-frame, $\hat{\omega}_{ie}^n$, and the angular rate measured by gyroscope measurement, $\hat{\omega}_{ib}^b$. In addition, the perturbation model of $\hat{v}_{tip}^n$ can be obtained by perturbing the INS velocity $\hat{v}_{INS}^n$, rotation matrix $\hat{C}_b^n$ and gyroscope measurement $\hat{\omega}_{ib}^b$ assuming that l_{bT}^b is known precisely, as follows:

$$\hat{v}_{tip}^{n} = \delta v_{INS}^{n} - \left((\omega_{in}^{n}\times)\left[\left(\boldsymbol{C}_{\boldsymbol{b}}^{\boldsymbol{n}} l_{tip}^{b}\right)\times\right] + \left[\boldsymbol{C}_{\boldsymbol{b}}^{\boldsymbol{n}}\left(l_{tip}^{b}\times\omega_{ib}^{b}\right)\times\right]\right)\phi - \boldsymbol{C}_{\boldsymbol{b}}^{\boldsymbol{n}}\left(l_{tip}^{b}\times\right)\delta\omega_{ib}^{b} \tag{11}$$

Then, the design matrix $\mathbf{H}_{ZUPT}$ can be denoted as:

$$\mathbf{H}_{ZUPT} = \begin{bmatrix}\mathbf{0}_3 & \mathbf{I}_3 & \mathbf{H}_{Z1} & -\mathbf{C}_b^n\left(l_p^b\times\right) & \mathbf{0}_3 & \mathbf{H}_{Z2} & \mathbf{0}_3\end{bmatrix} \tag{12}$$

where $\mathbf{I}_3$ and $\mathbf{0}_3$ respectively denote the 3×3 identity matrix and zero matrix; $\mathbf{H}_{Z1}$ and $\mathbf{H}_{Z2}$ are 3×3 matrixes, which can be denoted as:

$$\begin{cases}\mathbf{H}_{Z1} = -(\omega_{ie}^{n}\times)\left[\left(\mathbf{C}_b^n l_p^b\right)\times\right] - \left\{\left[\mathbf{C}_b^n\left(l_p^b\times\right)\omega_{ib}^b\right]\times\right\} \\ \mathbf{H}_{Z2} = -\mathbf{C}_b^n\left(l_p^b\times\right)diag\left(\omega_{ib}^b\right)\end{cases}$$

Similarly, for position measurement from the RTK receiver that is used for CUPT in the EKF, the position measurement equation can be expressed as:

$$z_{CUPT} = \mathbf{D}_R(\hat{r}_{GNSS}^e - r_{GNSS}^e) = \mathbf{H}_{CUPT}x + n_r \tag{13}$$

where $\hat{r}_{GNSS}^e$ and r_{GNSS}^e are the coordinates (latitude φ, longitude λ, and height h) of the INS-indicated position at the GNSS receiver's antenna phase center (AOC) and the GNSS RTK positioning result at the AOC, respectively; $\mathbf{D}_R = diag(R_M + h,\ (R_N + h)cos\varphi,\ -1)$, where R_M and R_N are the radius of the meridian circle and prime vertical, respectively. Thus, the design matrix $\mathbf{H}_{CUPT}$ can be denoted as

$$\mathbf{H}_{CUPT} = \begin{bmatrix}\mathbf{I}_3 & \mathbf{0}_3 & \left(\mathbf{C}_b^n l_p^b\right)\times & \mathbf{0}_3 & \mathbf{0}_3 & \mathbf{0}_3 & \mathbf{0}_3\end{bmatrix} \tag{14}$$

The statistical model considering measurement noise is known to have a significant influence on the Kalman filter algorithm for the optimal estimation of the system states. For CUPT, the standard deviation (STD) of the GNSS position measurement noise can be obtained easily from the STD of RTK positioning, but for ZUPT, the determination of the STD is difficult in theory. In this paper, we empirically tune the optimal STD through trial and error by considering the root-mean-square error (RMSE) of the positioning errors from multiple tests. The final optimal STD of the virtual zero-velocity observation errors is set to 0.06 m/s.

2.2.3 RTS Smoothing

After the final CUPT in an open-sky area, a smoothing algorithm can be applied in postprocessing to obtain the global optimal estimated error states and further improve the overall positioning accuracy by performing corrections to the INS. In this paper, we apply the RTS algorithm for smoothing, which is a well-known fixed-interval smoother. The RTS algorithm is relatively simple to implement and does not require the application of a full-scale backward filter. Further details of the algorithm can be found in [18, 19]. The principle is written as follows:

$$\hat{x}_{k/N} = \hat{x}_{k/k} + \mathbf{D}_k(\hat{x}_{k+1/N} - \hat{x}_{k+1/k}) \tag{15}$$

$$\mathbf{P}_{k/N} = \mathbf{P}_{k/k} + \mathbf{D}_k(\mathbf{P}_{k+1/N} - \mathbf{P}_{k+1/k})\mathbf{D}_k^T \tag{16}$$

where the smoothing gain matrix $\mathbf{D}_k$ can be denoted as:

$$\mathbf{D}_k = \mathbf{P}_{k/k}\boldsymbol{\Phi}_k^T\mathbf{P}_{k+1/k}^{-1} \tag{17}$$

2.2 Error State Observability

Although the EKF and RTS are expected to reduce the INS error to a large extent, the observability properties of the system error state affected by system dynamics actually limit the performance of the EKF and RTS. Taking GNSS/INS integration as an example, if the carrier is moving without acceleration changes and the gyro is low-grade, the component of gyro bias in the direction of specific force is unobservable; thus, the heading error can increase significantly quickly with time [20].

In regard to the error state observability of the INS on the pole, the position error, velocity error and horizontal attitude error are considered to be observable to some extent with the assistance of RTK positioning in an open-sky area; in addition, the velocity error and horizontal attitude error are considered to be fully observable when aided by LA-ZUPT in GNSS-denied areas. However, the heading error may be unobservable by CUPT for RTK positioning without proper maneuvering that induces acceleration changes, resulting in poor performance of long-term navigation. In addition, when RTK positioning update is unavailable in GNSS-denied environments, the position error is not observable by LA-ZUPT. Furthermore, the position error may drift quickly without LA-ZUPT and CUPT during the pole flying phase (i.e., Phase 1 in Fig. 1) in GNSS-denied environments.

Considering the restricted observability properties of the aided INS, the heading error and positioning error are sensitive to INS initialization, especially the heading alignment. Consequently, it is necessary to initialize the INS well at the beginning and obtain sufficient EKF convergence after the GNSS outage at the end with the assistance of RTK positioning. In addition, it is vital to apply RTS smoothing, which utilizes the available RTK position and the heading constraint on both sides of the GNSS outage to better estimate the unobservable INS error states and thus obtains better positioning of the target points, noting that they may be located in the middle of the GNSS-denied area. From the spatial optimization point of view, the starting point and the end point should be located on different sides of the target point to obtain the best geometric constraint if feasible for the application scenario. In addition to the forward survey trajectory, a return trajectory can be added to counteract the position measuring error related to heading errors and further improve the accuracy and robustness of the surveying to the target point.

3 EXPERIMENTS AND RESULTS

3.1 Experiment Description

Field tests were conducted on a campus playground in open-sky conditions to validate the feasibility and performance of the proposed solution, which aims to extend the RTK positioning capability to GNSS-denied areas. The choice of the open-sky condition is reasonable because it ensures good observation conditions for GNSS RTK. It is favorable for obtaining the ground truth using the integrated GNSS/INS reference system and obtaining the reference truth coordinates of the target points measured accurately by traditional RTK survey in advance. The GNSS-denied cases were simulated by discarding the RTK positioning update manually in the subsequent aided INS data processing.

Datasets were collected using the assembled pole as shown in Fig. 4 (a), which has a GNSS antenna mounted at the top end, a MEMS INS/GNSS integrated system set up on the aluminum plate mounted in the middle of the pole and a mechanical trigger mounted at the bottom tip. A quasi-tactical grade INS/RTK system was also attached on the aluminum plate to provide a reference truth for the navigation information. The MEMS INS/GNSS integrated system used in the experiment is *INS-Probe*, developed by the *i2Nav Group* of the *GNSS Research Center at Wuhan University*, which uses a dollar-level MEMS IMU chip, an ICM-20602 from *InvenSense*. Furthermore, connected to and synchronized with the *INS-Probe*, the mechanical trigger is responsible for accurate detection when the pole tip is in contact with the solid ground; in other words, the switch is toggled on once the pole tip lands on the ground and is toggled off once it is lifted off the ground, as shown in Fig. 4 (b)**.** The specifications of the instrument are listed below:

- IMU (embedded in the *INS-Probe*): *InvenSense ICM-20602*, a dollar-level MEMS IMU chip with gyroscope noise of 0.24 $\mathrm{deg}/\sqrt{h}$ and accelerometer noise of 100 $\mu\mathrm{g}/\sqrt{Hz}$, sampling at 200 Hz.
- Trigger: A mechanical switch serving as the pole tip zero-velocity detector.
- GNSS receiver: Two *NovAtel OEM719D* GNSS receivers serving as the rover and base station for the RTK.
- GNSS antenna: A *NovAtel GPS-7-2GGL* antenna and a u-blox ANN-MB multiband GNSS antenna.
- INS/RTK reference system: A quasi-tactical IMU module and u-blox GNSS module, providing position reference at centimeter level and heading reference accurate to 0.2° in postprocessing mode.

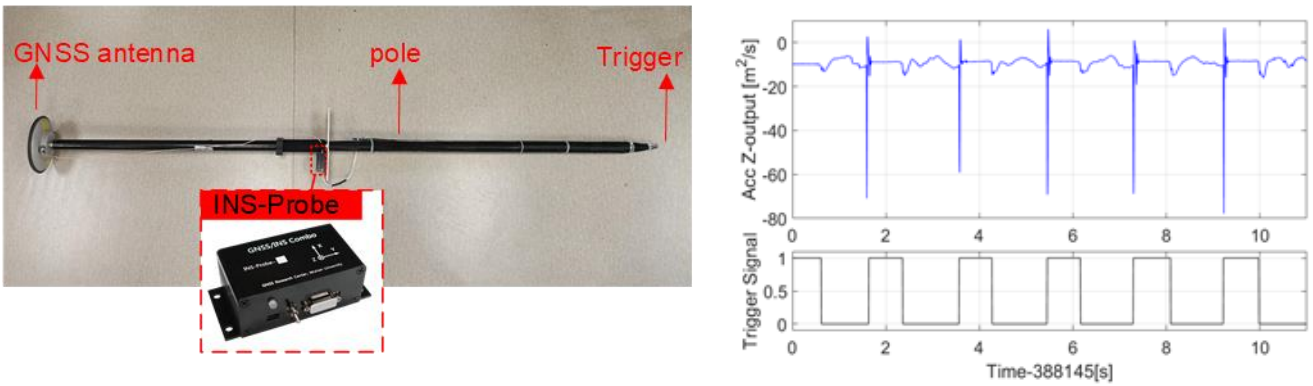

(a) Photograph of the inertial-aided positioning pole prototype (b) Diagram of ground contacts detected by the trigger

Fig. 4 The inertial-aided positioning pole with a trigger detecting ground contact

As described in Section 2.2, the straight-line trajectory (i.e., 'I' shape) is the best trajectory for obtaining an accurate result under good constraints provided by the high-quality positioning result at the beginning and ending points outside of the GNSS-denied area; in addition, the shorter the trajectory in the GNSS-denied area is, the better the positioning result that may be obtained. Considering that the GNSS-friendly spots close to the target point vary greatly in terms of distance and distribution in reality, three typical classes of trajectories (i.e., 'I'-shaped, 'L'-shaped and 'U'-shaped trajectories), and the I-shaped trajectory with the GNSS gap length varying from 100 meters to 20 meters are investigated individually. The designed trajectory with different distances is illustrated in Fig. 5. Note that the GNSS gap length refers to the length of the trajectory through the simulated GNSS-denied area in this study, and the effective RTK extension distance is actually half of the GNSS gap length. The target point is set at the center of the GNSS-denied trajectory, which has the greatest distance to the GNSS-friendly spots on both sides and benefits least from RTK positioning by RTS smoothing (i.e., it is the worst situation).

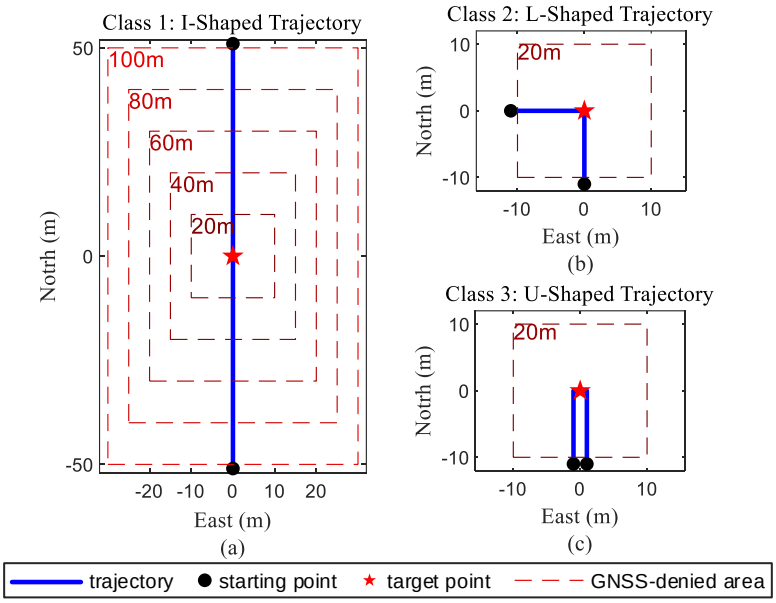

Fig. 5 Diagram of the designed trajectories with 3 different shapes through the GNSS-denied area in this study

In accordance with the designed surveying workflow, the datasets were collected with the following procedures: 1) Initialize the INS by sufficient movement of the pole at the starting point. 2) Walk along the designed trajectory toward the target point, manipulating the pole as a walking stick as if in a GNSS-denied environment and controlling the flying phase of the pole to be as short as possible (not exceed 2 seconds, averagely). 3) Reach the target point and obtain a measurement with the pole tip landing on the target. 4) Continue walking along the designed trajectory in walking stick mode until the ending point is reached, and maneuver the pole

sufficiently for approximately 1 minute. 5) Reverse the starting point and the ending point to walk along the reverse trajectory for another round of measurement. In the tests, the surveyor walked back and forth along the 100-meter I-shaped trajectory, obtaining measurements of the target point 30 times, and these data were processed with different simulated GNSS gap lengths in Cases 1~5 (Group 1) to investigate the influence of trajectory distances in GNSS-denied areas. In addition, the L-shaped trajectory and U-shaped trajectory datasets were collected similarly 19 times and 17 times, respectively, in Cases 5~7 (Group 2) to investigate the influence of the trajectory shapes under the same 20-meter GNSS gap length. The specification of these data processing cases is listed in **Table 1**.

Table 1 The data processing cases in this study

Index	Shape of trajectory	GNSS gap length	Repetitions	Result Group 1	Result Group 2
Case 1	I shape	100 m	30	●	
Case 2	I shape	80 m	30	●	
Case 3	I shape	60 m	30	●	
Case 4	I shape	40 m	30	●	
Case 5	I shape	20 m	30	●	●
Case 6	L shape	20 m	19		●
Case 7	U shape	20 m	17		●

3.2 Effects of LA-ZUPT and Smoothing

To investigate the benefits and limitations of LA-ZUPT in INS-based EKF and RTS smoothing, a typical example of Case 1 with an I-shaped trajectory and a 100 m GNSS gap (a 140 s GNSS outage) is studied using the ground truth from the INS/RTK reference system as a reference. Note that the INS was initialized well at the beginning, and the test data were processed in the following four modes:

1) INS/RTK filtering (EKF) without LA-ZUPTs
2) INS/RTK filtering (EKF) with LA-ZUPTs
3) INS/RTK smoothing (RTS) without LA-ZUPTs
4) INS/RTK smoothing (RTS) with LA-ZUPTs

Fig. 6 presents the navigation results of the inertial-aided positioning pole in the mentioned example, which are postprocessed in the above four modes. The GNSS outage started at 5 s and ended at 145 s. The two subfigures show the error plots of the filtering and smoothing results; each subfigure includes the modes without and with LA-ZUPT; and each mode shows plots of the position errors, velocity errors, roll & pitch errors, and heading errors. The errors along different directions are distinguished by color.

From Fig. 6 (a), the EKF performance with and without LA-ZUPT shows that 1) the pure INS drift is significant during the GNSS outage without any external measurement, but with the assistance of RTK positioning for CUPT in the INS-based EKF at the ending point, INS errors were reduced to some extent, except for the heading error due to insufficient movement of the pole at the end; and 2) it is apparent that LA-ZUPT during GNSS outage can greatly reduce the velocity errors as well as horizontal attitude errors and can thus restrict the drift of INS position errors so that it is slower compared with that of INS without LA-ZUPT, but this does not help in heading error estimation. From Fig. 6 (b), the RTS performance with and without LA-ZUPT shows that 1) although RTS smoothing may be able to reduce the INS-alone positioning errors from hundreds of meters to several meters, the additional aid of LA-ZUPT with the INS is still significant and promising for further improving INS positioning accuracy to the decimeter level; and 2) after LA-ZUPT and RTS smoothing, the largest attitude error appears in the heading estimate, which seems to drift over time; correspondingly, the positioning error is largest along the west-east direction, which is the transverse direction of the trajectory and is vulnerable to heading error, and the same is true for the velocity error. This shows that the heading error is the dominant error source, and it is possible to obtain better positioning results by improving the heading accuracy at the beginning and end of the GNSS outage. In conclusion, the low-cost INS results greatly benefit from LA-ZUPT in GNSS outages and from RTS smoothing, which takes full advantage of RTK positioning at the starting and ending points. Now that the position error seems to be closely related to the heading error, the heading error should be considered a key issue to be addressed in the proposed RTK extension solution.

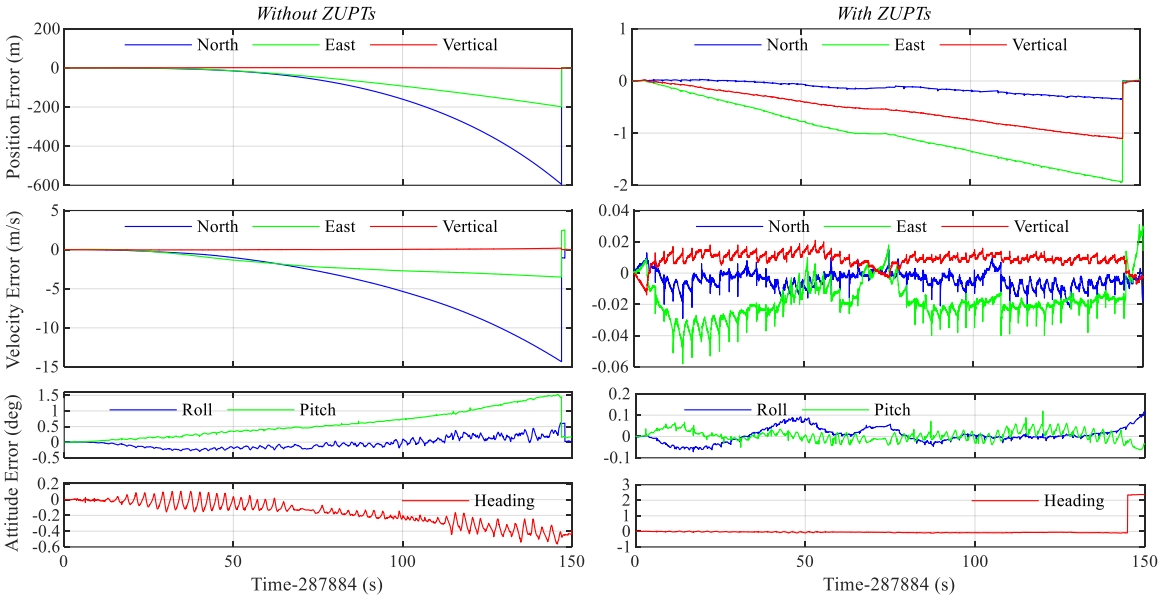

(a)EKF

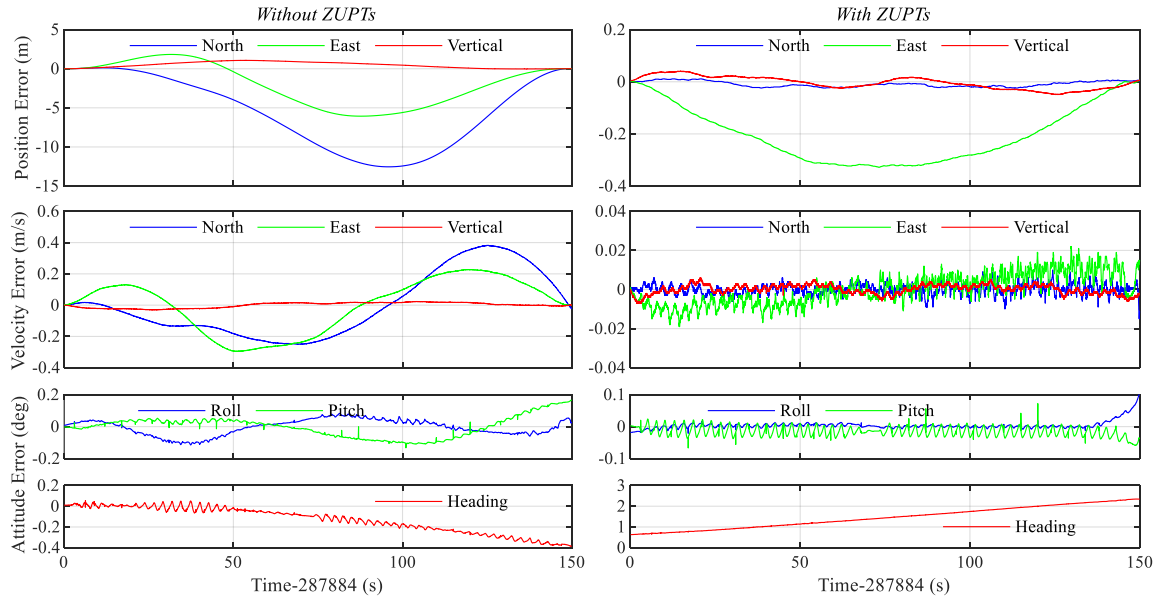

(b)RTS

Fig. 6 Comparison of the INS navigation errors between four different data processing modes. (Note that the assistance of RTK positioning is available at the beginning and end for only a few seconds.)

To mitigate the impact of the heading error, sufficient maneuvers can be provided at the starting and ending points to make the heading estimation converge using RTK positioning updates, as mentioned in Section 2.2. To investigate the positioning performance of the aided INS with improved headings, a few minutes of pole maneuvering at the ending point is added in data processing, and the errors of the estimated results are shown in Fig. 7. The heading error is further reduced in the EKF and RTS, and thus, the maximum position error of the INS after RTS smoothing is reduced from 0.3 m to 0.15 m, which confirms the link between the heading error and transverse positioning error in the smoothing result.

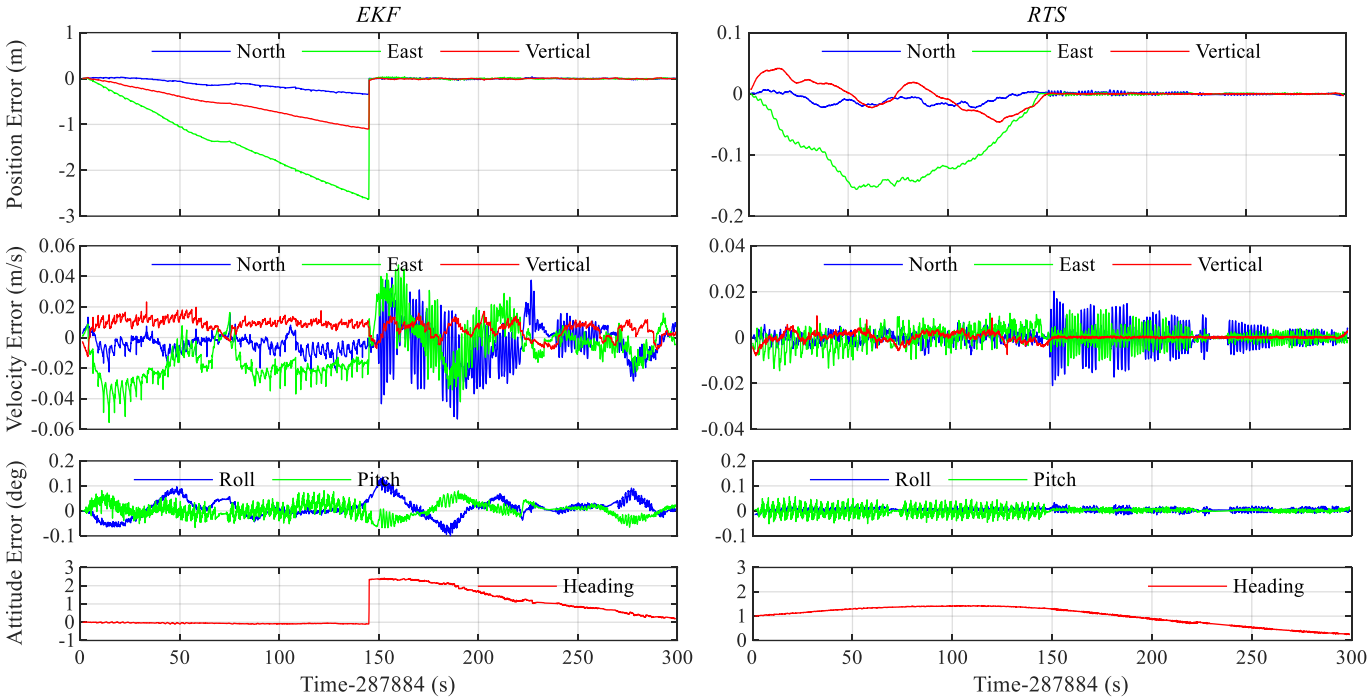

Fig. 7 INS result aided by LA-ZUPT and RTK positioning with heading convergence at the end. (Note that the assistance of RTK positioning is not only available at the beginning but also at the end with sufficient maneuvering to make the INS heading converge.)

3.3 Positioning Performance Analysis

According to Section 3.2, the INS error is reduced by LA-ZUPT and the position and heading constraints on both sides of the GNSS outage depend on RTS smoothing. Then, the shape of the trajectory (i.e., the geometric constraints in Section 2.2) and the GNSS gap length are expected to be the two main factors that impact the performance of the RTK extension solution. This section will investigate cases in Group 1 and Group 2 using the aforementioned surveyed reference truth coordinates of the target points to evaluate the positioning performance of the proposed RTK extension solution.

3.3.1 Performance with Different GNSS Gap Lengths

Since the GNSS gap length is supposed to be an important factor that influences the positioning performance, Cases 1~5 in Group 1 with different GNSS gap lengths varying from 100 m to 20 m, as described in Fig. 5, are investigated. The positioning errors are plotted in Fig. 8, and the corresponding statistical values are listed in Table 2.

As shown in Table 2 and Fig. 8, the positioning errors have similar characteristics to the plots in Figs. 6 and 7. There are some points with larger position errors distributed in the transverse direction (i.e., west-east) than in other directions (i.e., the heading direction and height direction) considering the RMSE in Cases 1~4, which can be affected by the estimated heading accuracy. As the length of the GNSS gap is reduced, the position accuracy, denoted as the RMSE, is improved in three dimensions; when the distance is shorter than 60 m, such as in Cases 3~5, the positioning accuracy is at the centimeter level considering the RMSE. Furthermore, in Case 5, with a 20-meter GNSS gap length, the pole tip maximum 3D positioning error is less than 7 cm, and the RMSE is smaller than 2 cm, which is close to the real RTK survey accuracy. These test results showed that the feasibility of the proposed RTK extension solution with a short GNSS gap length is confirmed to attain centimeter-level positioning accuracy, so it can be applied in various scenes, such as surveys in small buildings and under bridges, overpasses, or dense canopies.

Table 2 Positioning errors of the target point measured by the inertial pole experiencing different GNSS gap lengths

Unit: meters	Case 1 (100 m)			Case 2 (80 m)			Case 3 (60 m)			Case 4 (40 m)			Case 5 (20 m)		
	N	E	H	N	E	H	N	E	H	N	E	H	N	E	H
RMSE	0.049	0.154	0.038	0.031	0.108	0.029	0.024	0.061	0.026	0.022	0.037	0.021	0.019	0.019	0.014
MEAN	-0.005	-0.008	0.000	-0.002	0.015	-0.003	-0.004	0.014	0.007	-0.002	0.011	0.003	-0.004	0.007	0.001
MAX	0.101	0.391	0.094	0.059	0.312	0.061	0.045	0.159	0.061	0.031	0.101	0.063	0.021	0.035	0.027

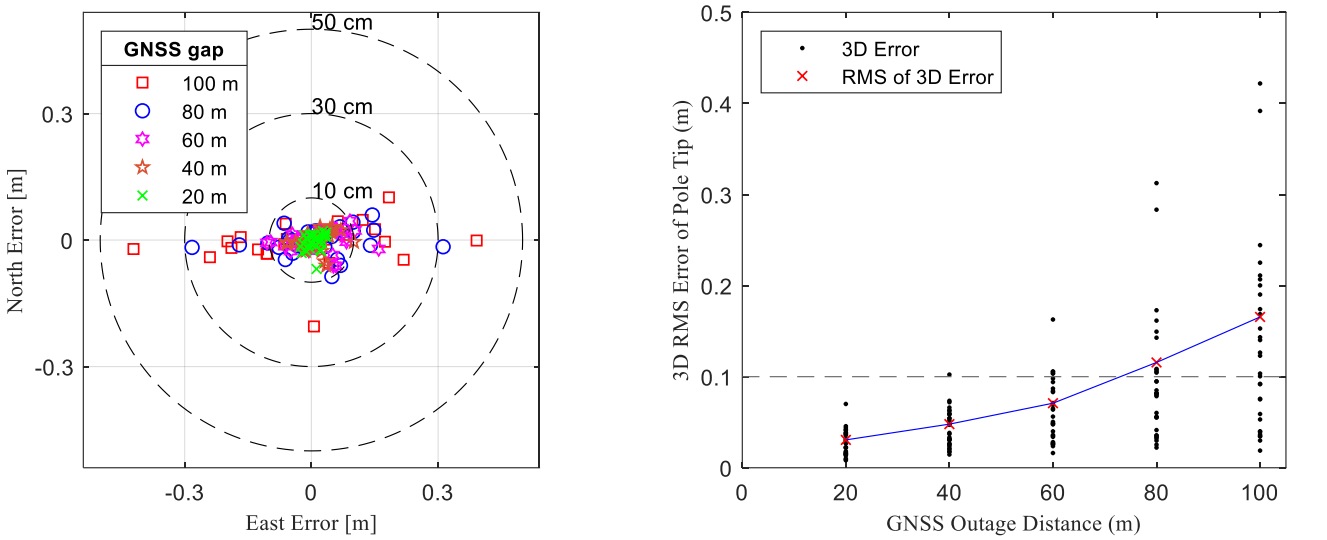

(a) Horizontal positioning error distribution

(b) Correlation of the positioning accuracy with the GNSS gap length

Fig. 8 The positioning error of the proposed RTK extension solution in Cases 1~5

3.3.2 Performance with Different Trajectory Shapes

Considering that GNSS-friendly spots that are close to the target point may be limited in reality, the influence of the location of the starting point and the ending point is investigated. In Group 2, Cases 5~7 with typical trajectories in I, L, and U shapes are tested, among which the I-shaped trajectory is supposed to provide the best constraint on position error in the transverse direction and on heading error, but the L-shaped and U-shaped trajectories are more flexible and applicable in a variety of GNSS-denied scenes.

Table 3 and Fig. 9 compare the horizontal position error distributions among Cases 5, 6, and 7. The results show that 1) the horizontal position error is generally more biased in Cases 6~7 than Case 5; 2) Case 7, with the U-shaped trajectory, is the worst with a discrete distribution, which is explainable for weaker geometric constraints in terms of position and heading. However, for Case 6, with an L-shaped trajectory, the maximum 2D position error is still less than 12 cm, and the RMSE is less than 6 cm in the three dimensions of position, which may still be feasible and applicable for the specific needs of surveying.

Table 3 Positioning errors of the target point measured by the inertial pole with different trajectory shapes

Unit: meters	Case 5 (I-shaped)			Case 6 (L-shaped)			Case 7 (U-shaped)		
	N	E	H	N	E	H	N	E	H
RMSE	0.019	0.019	0.014	0.053	0.056	0.026	0.038	0.111	0.047
MEAN	-0.004	0.007	0.001	0.033	-0.049	0.021	-0.017	-0.083	-0.014
MAX	0.021	0.035	0.027	0.11	0.008	0.046	0.043	0.115	0.081

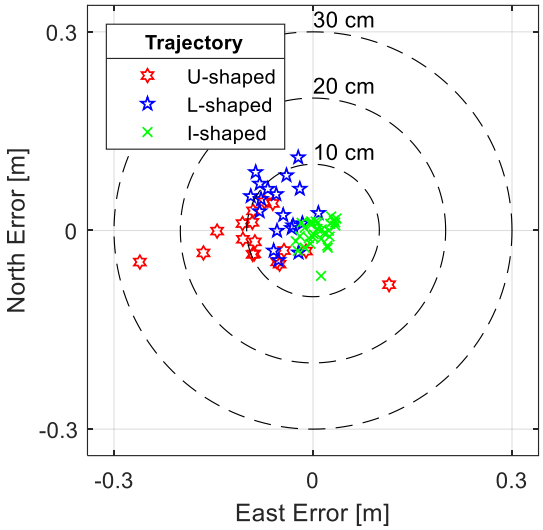

Fig. 9 Horizontal positioning error distribution in Cases 5~7

3.3.2 Performance with a Back-and-Forth Combination

Noting that the horizontal position errors of Cases 1~5 with an I-shaped trajectory follow an axisymmetric distribution, it is worth combining (i.e., averaging) the two adjacent positioning results of the same target point measured by going back and forth along the I-shaped trajectory. Thus, the 30 measurements are divided into 15 groups, in which two position measurements complete a back-and-forth loop and the combination of forward and reverse measurements is obtained for higher accuracy and robustness. Fig. 10 and Table 4 show that the overall position error is significantly reduced, by more than 40%, for all cases in terms of RMSE and maximum error. In Cases 3~5 with GNSS gaps of no more than 60 m, the RMSE is approximately 5 cm with a maximum error not exceeding 10 cm, which means that it is feasible to obtain more accurate and robust results by combining the back-and-forth measurements, sacrificing half of the operational efficiency.

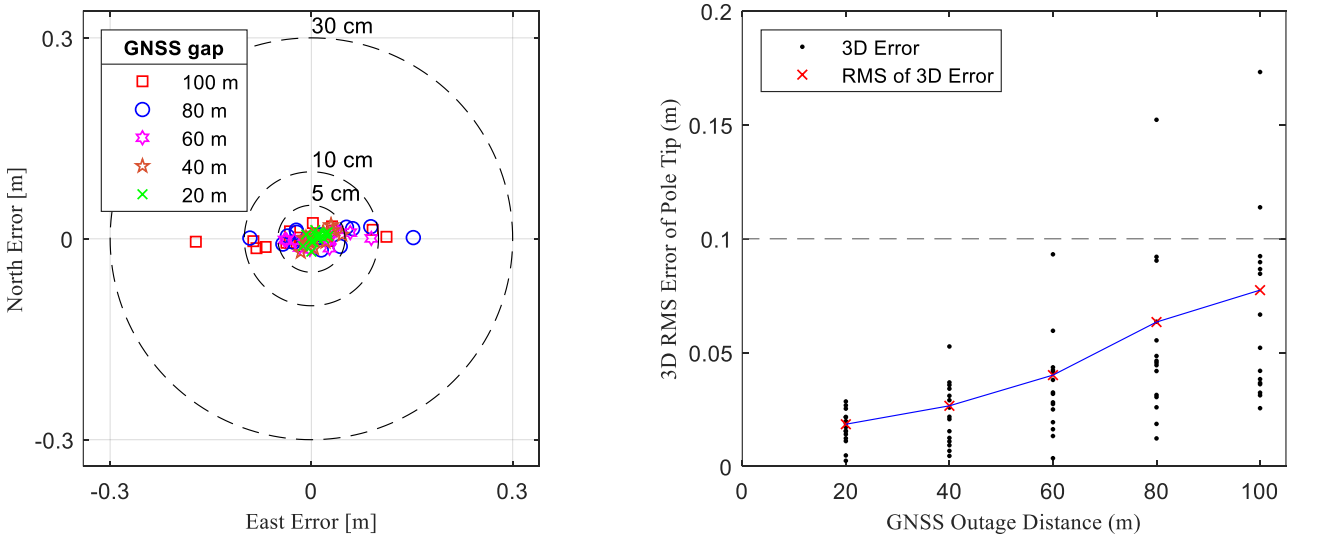

(a) Horizontal positioning error distribution (b) Correlation of positioning accuracy with GNSS gap length

Fig. 10 The positioning error of the RTK extension solution with a back-and-forth combination in Cases 1~5

Table 4 Positioning errors of the target point measured by the inertial pole with the back-and-forth combination

Unit:	Case 1 (100 m)			Case 2 (80 m)			Case 3 (60 m)			Case 4 (40 m)			Case 5 (20 m)		
meters	N	E	H	N	E	H	N	E	H	N	E	H	N	E	H
RMSE	0.011	0.071	0.028	0.011	0.059	0.019	0.008	0.036	0.015	0.011	0.02	0.013	0.008	0.014	0.009
MEAN	0.002	-0.017	-0.014	0.003	0.012	-0.011	-0.001	0.01	0.003	0.002	0.009	0.000	0.001	0.008	0.001
MAX	0.023	0.112	0.024	0.018	0.152	0.013	0.013	0.089	0.026	0.02	0.046	0.025	0.013	0.025	0.013

4 CONCLUSION

To extend RTK survey capabilities to GNSS-denied areas at an acceptable cost, this paper proposes an RTK extension solution using a low-cost inertial-aided positioning pole operated in walking stick mode. The solution uses a dollar-level MEMS IMU fixed on the RTK survey pole to run the inertial navigation aided by 1) the LA-ZUPT when the pole tip touches the ground regularly, which effectively reduces the velocity error and the horizontal attitude error and slows the position drift significantly; 2) the CUPT provided by RTK positioning at the starting and ending points around the target point, which is processed by the EKF and RTS smoothing algorithms and provide strict geometric constraints for the INS position drift; and 3) the accurate heading constraint at the starting and ending points, which is obtained by enhancing the heading observability through sufficient maneuvering of the pole with the RTK positioning update. Considering the availability of open-sky areas around the target point, i.e., the geometry of the starting and ending point distribution, different lengths of trajectories, including I-shaped, L-shaped and U-shaped trajectories, are tested to validate the feasibility and performance of this RTK survey-extending solution in a comprehensive way. The experimental results with multiple datasets illustrate that the I-shaped trajectories under 40 m and the L-shaped trajectories of 20 m are advantageous for obtaining centimeter-level positioning in terms of RMSE, and by combining (i.e., averaging) the two positioning results measured along the back-and-forth I-shaped trajectories, the combined result becomes more accurate and robust, with the RMSE and maximum error reduced by more than 40%. The proposed low-cost RTK extension solution using an inertial-aided positioning pole is validated to be feasible and can meet the requirements for extending the RTK survey capability to GNSS-denied areas for certain distances.

Future work will focus on further improvements to the RTK extension solution, including 1) a thorough theoretical analysis of INS error observability to optimize the hardware design, operation procedures, and algorithm parameters, 2) quality control for the multisensor integration algorithm and an integrity study of the system, and 3) replacement of the mechanical trigger by automatic detection based on IMU data.

ACKNOWLEDGMENTS

The authors would like to express our sincere gratitude to Prof. Xiaoji Niu and Dr. Qijin Chen for supervising the research in this paper and for their constructive suggestions and encouragement. In addition, we would like to thank Dr. Kuang Jian and Yu Li, who motivated the idea of ZUPT with lever-arm compensation, and Dr. Tisheng Zhang and Hailiang Tang for providing the GNSS/INS system (i.e., *INS-Probe*) used in the experiment. The authors also gratefully acknowledge the research grant support provided by *The National Key Research and Development Program of China* (No. 2016YFB0502202) and *the National Natural Science Foundation of China* (41904019).

REFERENCES

[1] P. Teunissen and O. Montenbruck, *Springer Handbook of Global Navigation Satellite Systems*, 1st ed. 2017. ed. (Springer Handbooks). Springer International Publishing, 2017.

[2] X. Luo, S. Schaufler, M. Carrera, and I. Celebi, "High-Precision RTK Positioning with Calibration-Free Tilt Compensation," presented at the FIG Congress 2018, Istanbul,Turkey, May 6-11, 2018.

[3] K. J. R. o. G. Schwarz, "Inertial surveying and geodesy," vol. 21, no. 4, pp. 878-890, 1983.

[4] Q. Chen, X. Niu, Q. Zhang, and Y. J. N. J. o. T. I. o. N. Cheng, "Railway track irregularity measuring by GNSS/INS integration," vol. 62, no. 1, pp. 83-93, 2015.

[5] Q. Chen *et al.*, "A railway track geometry measuring trolley system based on aided INS," *Sensors,* vol. 18, no. 2, p. 538, 2018.

[6] M. S. Chowdhury and M. F. Abdel-Hafez, "Pipeline inspection gauge position estimation using inertial measurement unit, odometer, and a set of reference stations," *ASCE-ASME Journal of Risk and Uncertainty in Engineering Systems, Part B: Mechanical Engineering,* vol. 2, no. 2, pp. 021001-1, 2016.
[7] H. Sahli and N. El-Sheimy, "A novel method to enhance pipeline trajectory determination using pipeline junctions," *Sensors,* vol. 16, no. 4, p. 567, 2016.
[8] Q. Chen, X. Niu, J. Kuang, and J. Liu, "IMU Mounting Angle Calibration for Pipeline Surveying Apparatus," *IEEE Transactions on Instrumentation and Measurement,* vol. 69, no. 4, pp. 1765-1774, 2020.
[9] E. Foxlin, "Pedestrian tracking with shoe-mounted inertial sensors," *IEEE Computer graphics and applications,* no. 6, pp. 38-46, 2005.
[10] S. K. Park and Y. S. Suh, "A zero velocity detection algorithm using inertial sensors for pedestrian navigation systems," *Sensors,* vol. 10, no. 10, pp. 9163-9178, 2010.
[11] M. Ren, K. Pan, Y. Liu, H. Guo, X. Zhang, and P. Wang, "A novel pedestrian navigation algorithm for a foot-mounted inertial-sensor-based system," *Sensors,* vol. 16, no. 1, p. 139, 2016.
[12] X. Niu, Y. Li, J. Kuang, and P. Zhang, "Data Fusion of Dual Foot-Mounted IMU for Pedestrian Navigation," *IEEE Sensors Journal,* vol. 19, no. 12, pp. 4577-4584, 2019.
[13] B. R. H. Scherzinger, CA), "Walking stick navigator for position determination," United States, 2005. Available: https://www.freepatentsonline.com/6853909.html.
[14] B. M. R. H. Scherzinger, CA), "AINS enhanced survey instrument," United States, 2009. Available: https://www.freepatentsonline.com/y2009/0024325.html.
[15] Q. Chen, H. Lin, R. Guo, and X. Niu, "Rapid and accurate initial alignment of the low-cost MEMS IMU chip dedicated for tilted RTK receiver," *GPS Solutions,* vol. 24, no. 4, 2020.
[16] E.-H. Shin, "Estimation techniques for low-cost inertial navigation," *PhD Thesis, University of Calgary,* vol. 20219, 2005.
[17] P. S. Maybeck, *Stochastic models, estimation, and control*. Academic press, 1982.
[18] P. S. Maybeck, *Stochastic models, estimation, and control*. Academic press, 1982.
[19] H. E. Rauch, F. Tung, and C. T. Striebel, "Maximum likelihood estimates of linear dynamic systems," *AIAA journal,* vol. 3, no. 8, pp. 1445-1450, 1965.
[20] S. Hong, M. H. Lee, H.-H. Chun, S.-H. Kwon, and J. L. Speyer, "Observability of error states in GPS/INS integration," *IEEE Transactions on Vehicular Technology,* vol. 54, no. 2, pp. 731-743, 2005.